Open Access Library Journal
2023, Volume 10, e10270
ISSN Online: 2333-9721
ISSN Print: 2333-9705

Topology-Optimized and Simulation-Driven Design for Compact Autonomous Electric Vehicle Drive Systems: A Novel Approach

Qasim M. Ajao[1*], Lanre G. Sadeeq[1], Olukotun Oludamilare[1], Steven Letendre[2]

[1]Department of Electrical Engineering, Georgia Southern University, Statesboro, Georgia, USA
[2]Microsoft Corporation, Redmond, Seattle, Washington DC, USA
Email: *Qasim.ajao@ieee.org

How to cite this paper: Ajao, Q.M., Sadeeq, L.G., Oludamilare, O. and Letendre, S. (2023) Topology-Optimized and Simulation-Driven Design for Compact Autonomous Electric Vehicle Drive Systems: A Novel Approach. *Open Access Library Journal*, **10**: e10270.
https://doi.org/10.4236/oalib.1110270

Received: May 18, 2023
Accepted: June 27, 2023
Published: June 30, 2023

Copyright © 2023 by author(s) and Open Access Library Inc.
This work is licensed under the Creative Commons Attribution International License (CC BY 4.0).
http://creativecommons.org/licenses/by/4.0/

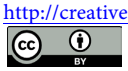

Open Access

Abstract

This paper introduces a novel approach to drive system design for compact autonomous electric vehicles (AEVs) by utilizing topology optimization and simulation techniques. The primary goal is to develop an efficient and lightweight drive system that improves vehicle performance, taking into account the specific requirements of autonomy and electric propulsion. The design process incorporates topology optimization to systematically explore different configurations and material distributions, with the aim of maximizing structural integrity and efficiency. Simulation tools are employed to evaluate performance and validate the optimized design. The results demonstrate the effectiveness of this methodology in creating an optimized drive system that meets the needs of compact AEVs. Furthermore, this study focuses on the motor-drive axle integrated driving scheme to enhance the driving efficiency of AEVs. The paper addresses this challenge by carefully considering power matching and transmission ratio calculations based on the performance characteristics of compact AEVs, resulting in a determined total gear ratio of 8.124. To further enhance overall performance & efficiency, a 2-stage retarder system is developed.

Subject Areas

Electric Engineering

Keywords

Autonomous Electric Vehicles, EV Drive Simulation, Drive Cycles, Self-Driving Vehicles, Stress Simulation, Topology, Optimize Drive

1. Introduction

The increasing advancements in technology have underscored the need for innovative drive system designs tailored to compact autonomous electric vehicles (AEVs). The drive system significantly impacts performance metrics such as energy efficiency, maneuverability, and dependability. However, designing optimal drive systems for these vehicles is challenging due to constraints in size, weight, and power. To address these challenges, this paper proposes a synergistic approach that combines topology optimization and simulation techniques to achieve efficient and lightweight drive system designs. In the context of global concerns regarding energy conservation and environmental preservation, there is a growing emphasis on developing and implementing energy-saving and emission-reducing technologies across industries. The automotive sector, in particular, is focused on reducing carbon emissions, with a specific focus on fossil fuels [1] [2] [3].

Energy-saving and emission-reducing technologies are at the forefront of vehicle development, with research institutions and automakers prioritizing the field of new energy vehicles. AEVs offer numerous advantages over traditional fossil fuel-powered vehicles, including zero carbon emissions, versatile applications, and promising market prospects. Significant progress has been made in advancing AEV technologies within the automotive industry. The drive system, a crucial component of AEVs, directly influences their performance and efficiency, highlighting the importance of optimizing it, particularly in terms of compactness for better integration with the propulsion motor. Research has revealed that compared to gasoline-powered vehicles, AEVs often feature simpler and more compact drive systems. Using this information as a foundation, this research study focuses on reducing the size and weight of the drive system to improve transmission efficiency, lower energy use, and guarantee reliability [3]. We created and improved the transmission system of AEVs by reducing the weight of transmission modules to fulfill certain criteria and enhance the dynamic performance of the cars, drawing on prior research.

2. Developing and Matching the Driven Parameters

The implementation of the partial transmission scheme in AEVs is characterized by a straightforward design that employs a centralized-driven approach with a single reduction gear. The scheme's ability to achieve the desired driving cycle is highly dependent on effective motor speed regulation, which plays a crucial role in optimizing the dynamic performance of the vehicle. To address the issue of under-performance at medium-high speeds in electric vehicles, researchers have investigated the integration of a two-stage retardation method into the power transmission system.

2.1. Specification and Synchronization of Driving Motor

Self-driving electric vehicles currently use a variety of electric motor types, in-

cluding DC motors, AC asynchronous motors, permanent-magnet synchronous machines, and switching reluctance machines. These motors each have unique qualities. In the beginning, DC motors were used in AEVs; but, because of their complicated and bulky structures, as well as the requirement for regular and expensive maintenance, these motor types have gradually decreased in use.

Despite their relative weakness in terms of constant power factor, permanent-magnet synchronous machines stand out among AC motors due to their competitive overload capacity, higher load efficiency, and superior power factors in comparison to other solutions. Our study, however, concentrated on optimizing the advantages of the permanent-magnet synchronous machine, including its small size, remarkable torque performance, high efficiency, and dependability.

2.2. Power Compatibility

The role of the driving motor in vehicle performance is widely recognized. Motors with insufficient power lack the necessary dynamic properties, resulting in prolonged overloading and a detrimental impact on their lifespan. However, it is important to note that high-power motors, while offering a significant reserve capacity, come with the trade-off of increased weight and size. This can have a negative impact on the overall efficiency of AEVs and make them less cost-effective [4].

When considering a motor for AEVs, it is critical to consider a variety of characteristics, which includes the motor's rated output, peak power, rated revolution, and peak performance revolution. The rated output, together with the peak power of the motor, is defined to ensure uninterrupted operation even at the vehicle's highest speed. Moreover, factors like rolling resistance and air resistance become significant when the vehicle is in motion. Taking all these factors into account, the power required by the vehicle at its maximum speed ($V_{\max}$) can be calculated using the following formula:

$$P_{V_{\max}} = \left(mgf + \frac{C_D A V_{\max}^2}{21.15} \right) \frac{V_{\max}}{3600\eta_T}. \quad (1)$$

The formula comprises several variables:

- m denotes the complete vehicle curb mass (kg).
- g represents gravitational acceleration (m/S^2).
- f represents the coefficient of rolling resistance.
- C_D represents the coefficient of air resistance.
- A represents the frontal area.
- $V_{\max}$ signifies the maximum speed (km/h).
- η_T denotes transmission efficiency.

It is of the most crucial importance to ensure that the driving motor of AEVs delivers at least 90 percent of the power essential to attain the vehicle's top speed on a level road. In other terms, the minimum power required for AEVs to attain their optimum speed on a level road is the lesser of their rated power and re-

quired power [5].

$$P_{mas} \geq \max\left(P_{V_{\max}}, P_{i_{\max}}, P_t\right). \tag{2}$$

Furthermore, when the power demands of vehicle accessories are taken into consideration, the final calculated rated power is 20 kW, with a maximal power of 40 kW (as per Formula (2)). In addition to $V_{\max}$, maximal gradeability, and acceleration time, the following formula is employed to calculate the motor's maximum power. **Table 1** presents an inclusive compilation of the technical parameters and design requirements specific to a compact autonomous electric car. Besides accounting for rolling resistance and air resistance, it is essential to consider the influence of grade resistance. When the vehicle is traveling at a constant uphill speed of 25 km/h, the power needed can be determined by applying the following formula [6].

$$P_{i_{\max}} = \left(mgf\cos\alpha_{\max} + mg\sin\alpha_{\max} + \frac{C_D A V_s^2}{21.15}\right)\frac{V_s}{3600\eta_T}. \tag{3}$$

Within the equation, the symbol $V_{\max}$ signifies the maximum gradient angle, while V_s represents the stabilized speed in kilometers per hour (*km/h*). The acceleration time of the vehicle was specifically determined under level road conditions. Consequently, the power required for the acceleration time, excluding the influence of grade resistance, can be calculated using the subsequent equation.

$$P_t = \left(mgf + \frac{C_D A V^2}{21.15} + \delta m\frac{\mathrm{d}v}{\mathrm{d}t}\right)\frac{V}{3600\eta_T}. \tag{4}$$

In the given equation, the variable v represents the running speed (*km/h*),

Table 1. System parameters of autonomous EVs.

Attributes (Parameters)	Value
Complete vehicle curb mass (m)	950
Maximum loading capacity (kg)	210
Frontal area A (m^2)	1.94
The rolling radius of the tire R (m)	0.329
Transmission efficiency η_T	0.86
Coefficient of air resistance C_D	0.3
Correction coefficient of mass δ	1.04
Coefficient of rolling resistance f	0.011
Maximum speed $V_{\max}$	110 km/h
Maximum gradeability $i_{\max}$ 25 km/h	25%
Driving mileage S	150 km
Acceleration time (0 - 50 km/h)	8 s
Acceleration time (0 - 100 km/h)	14 s

while δ represents the correction coefficient of mass. With the objective to facilitate the calculation of the correlation between vehicle speed and acceleration time during the vehicle's transition from rest to acceleration, an equivalent fitting method has been implemented [4]. The simplified calculation, derived from this fitting technique, is expressed below:

$$V = V_m \left(\frac{t}{t_m} \right)^a . \tag{5}$$

Within the equation, V_m represents the speed at the conclusion of the acceleration phase, measured in kilometers per hour (km/h). The variable tm corresponds to the duration of acceleration, expressed in seconds (s), while the coefficient a serve as a fit parameter, commonly set to a value of 0.5. Equation (6), as provided below, is obtained by substituting Equation (5) for Equation (4).

$$P_t = \left(mgf \frac{V_m}{1.5} + \frac{C_D A V_m^3}{52.875} + \frac{\delta m V_m^2}{7.2 t_m} \right) \frac{1}{3600 \eta_T}. \tag{6}$$

Based on the acceleration times provided in **Table 1**, we selected V_m values of 50 km/h and 100 km/h, along with corresponding tm values of 8 s and 14 s. Through calculations, we determined that accelerating from 0 to 50 km/h requires 15.40 kW of power, while accelerating from 0 to 100 km/h necessitates 37.42 kW. To keep up maximum speed, a minimum motor power of 15.47 kW is necessary, while a minimum motor power of 19.21 kW is needed for climbing. In many different kinds of settings, the greatest power demand comes during acceleration. Considering an established overload capacity, Equation (2) mandates that the motor's peak output has to be at least 37.42 kW. In the case of AEV motors, their rated power values typically exceed 90% of the power required to reach the highest speed on a flat road [7]. In addition, consideration should be given to the power demands of accessories like air conditioners and electrical devices. Therefore, in this study, we considered the power necessary for the vehicle to achieve its maximum speed on a level road as the lower limit for the rated power of the driving motor, resulting in a minimum rated power of 15.47 kW.

2.3. Motor Alternatives

Permanent-magnet synchronous machines are commonly classified as medium-speed motors, typically operating within a speed range of 4000 to 10,000 r/min. The coefficient of expanded power zone, denoted as (β), is usually between 2 and 4 and represents the ratio of the motor's highest speed to its rated speed [4]. Higher maximum speeds of the driving motor require stricter production standards and result in higher costs. They also necessitate reinforced gear and bearing units in the transmission system, particularly in terms of resistance to impact and endurance against stress [8].

In this study, the initial rated speed of the motor is set at 2500 r/min, while the maximum speed is 8000 r/min, with a β value of 0.32. Under these defined con-

ditions, the driving motor has a rated power of 20 kW and a peak power of 40 kW. The calculated rated torque is 76 N*m, and the peak torque is 152 N*m. For more detailed information on the motor parameters, please refer to Table 2.

3. Approximate Design of Transmission Case

Transmission Scheme

The transmission options available for AEVs encompass the mechanical drive layout, motor-drive axle integral, and distributed layout. The mechanical drive layout is considered outdated, while achieving full implementation of the distributed electric drive remains challenging. Presently, the motor-drive axle combined scheme is widely embraced in AEVs due to its simplicity, high efficiency, and comparable driving performance to conventional fuel-powered cars. Companies choose this design because it allows for cost management and is often mounted on the front axle of the vehicle.

The transmission box provides a number of formulations within the motor-drive combination system, including the constant speed ratio retarder and multidrive. More gear-based multidrive systems can lengthen the motor's working life and boost the vehicle's economic and dynamic performance. But an excessive number of gears can complicate the transmission system, adding weight and cost [6].

In current AEVs, a two-speed transmission is commonly used as additional gears do not significantly improve performance beyond reducing efficiency. The transmission system is crucial for the dynamic properties and mechanical efficiency of AEVs. To tackle this challenge, fixed-speed ratio retarders are commonly employed in existing AEVs due to their simplicity, lightweight construction, compact size, and affordability. This retarder, in combination with a conventional differential, facilitates vehicle deceleration and increases torque.

To achieve cost reduction, the fixed speed ratio retarder is combined with a traditional differential to create a double reduction system consisting of four gears. Gear 4 is specifically integrated with the differential to minimize both size and weight. Splines are used to attach the motor to a high-speed shaft, allowing for backward motion via motor reversal. As shown in Figure 1, the bevel gear of the differential is mounted inside the retarder shell at the right end of the

Table 2. System parameters of driving motor.

Attributes (Parameters)	Value
Power (kW)	20
Peak (kW)	40
Speed (r/min)	2500
Peak Speed (r/min)	8000
Torque N*m	76
Peak Torque N*m	152

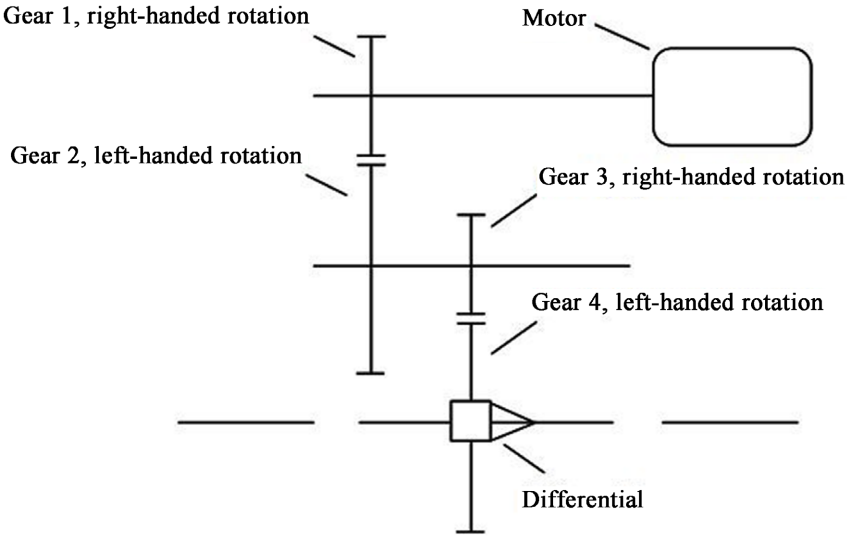

Figure 1. 2-Dimension of deceleration system.

integrated Gear 4-differential arrangement. This arrangement allows for splash lubrication. This configuration offers a compact structure that maximizes the low-speed torque capabilities of the chosen permanent magnet synchronous motor. This advantage is particularly beneficial for compact AEVs with lower dynamic properties [9].

The maximum transmission ratio allows the vehicle to sustain a constant climbing speed while the motor operates at its maximum torque, as shown below:

$$i_0 \cdot i_g \geq \frac{mgf\left(\cos\alpha_{\max} + \sin\alpha_{\max}\right) + \dfrac{C_D A V_m^3}{21.15}}{T_{\max} \cdot \eta_T}. \tag{7}$$

In the given equation, i_0 denotes the transmission ratio of the main retarder, i_g represents the transmission ratio of the differential, r signifies the rolling radius of the tire (m), and $T_{\max}$ represents the peak torque of the motor in (N*m). The vehicle's dynamics and economic performance are greatly influenced by the transmission ratio [10]. It is crucial to calculate the minimum and maximum values of this ratio to determine the ideal total transmission ratio. Additionally, it is crucial to ensure that the maximum driving force, as calculated by Formula (8), does not exceed the adhesive limit.

$$i_0 \cdot i_g \leq \frac{F_Z \cdot \phi \cdot r}{T_{\max} \eta_T}. \tag{8}$$

The formula includes the coefficient of adhesion ϕ (0.8 in this study) and the normal reaction F_Z of the ground to the driving wheel. After the calculations, the range of $i_{\max}$ is found to be between 5.987 and 9.373. Furthermore, the minimum transmission ratio is affected by the maximum speed and running resistance of the vehicle, as depicted in Formula (9).

$$i_0 \cdot i_g \geq \frac{0.377_r \cdot \eta_{\max}}{V_{\max}}. \tag{9}$$

The formula incorporates $\eta_{\max}$, which denotes the maximum speed of the motor, and $V_{\max}$, which signifies the maximum speed in kilometers per hour (km/h), and it is in compliance with the following formula [4] [5] [6].

$$i_0 \cdot i_g \geq \frac{\left(mgf + C_D A V_{\max}^3\right) \cdot r}{T_{\max} \cdot \eta_T}. \tag{10}$$

$$\begin{cases} 5.987 \leq i_{\max} \leq 9.373, \\ 1.096 \leq i_{\min} \leq 9.021. \end{cases} \tag{11}$$

The range for $i_{\min}$ is estimated to be between 1.096 and 9.021. The following formula can be used to fully reflect the proposed transmission ratio in the study. It's crucial to avoid employing small transmission ratios in the design to account for the driving motor's fast speed. According to the calculations described before, $i_{\max}$ should be restricted to 9.021, and $i_{\min}$ shouldn't be lower than 5.987. Consequently, 8.1 was chosen as the original transmission ratio. The two-stage transmission ratio adhered to the equal speed ratio idea [11].

4. Calculation of Parameters

Design and modeling of the transmission case involved determining the parameters for the first and second gears in the retarder, which were selected based on helical cylindrical gears. The specific values of these parameters can be found in **Table 3**. The first gearbox specifications are as follows, from the design manual: Gear 1 has 19 teeth, Gear 2 has 53 teeth, module size is 2.5 mm, center distance is 97 mm, helix angle is 21.90˚, reference diameters are 51.194 mm for Gear 1 and 142.805 mm for Gear 2, gear widths are 40 mm and 38 mm, and the transmission ratio is 2.789. (**Figure 2**)

Similarly, for the second gear, it is driven by a helical cylindrical gear with a pinion of 23 teeth (z_3), a rack wheel of 67 teeth (z_4), a face width coefficient of 0.7, a standard module of 3.0, a center distance of 146 mm, a helix angle of 22.392˚, a reference diameter of 74.627 mm for Gear 3, a reference diameter of 217.391 mm for Gear 4, gear widths of 60 mm for Gear 3 and 55 mm for Gear 4, and a transmission ratio of 2.913, (z_1 = 16, z_2 = 20, is depicted in **Table 4**). Furthermore, for compact AEVs, the planetary gear number is set to 2, and the

Table 3. System transmission parameters.

Attributes (Parameters)	Value
1st Transmission ratio	950
Motor (peak power) (kW)	210
Motor (peak torque) (N*m)	1.94
High Speed Shaft (Input Torque) (N*m)	0.329
High Speed shaft (Input Power) (kW)	0.86
Low Speed Shaft (Input Torque) (N*m)	0.3
Low Speed Shaft (Input Power) (kW)	1.04

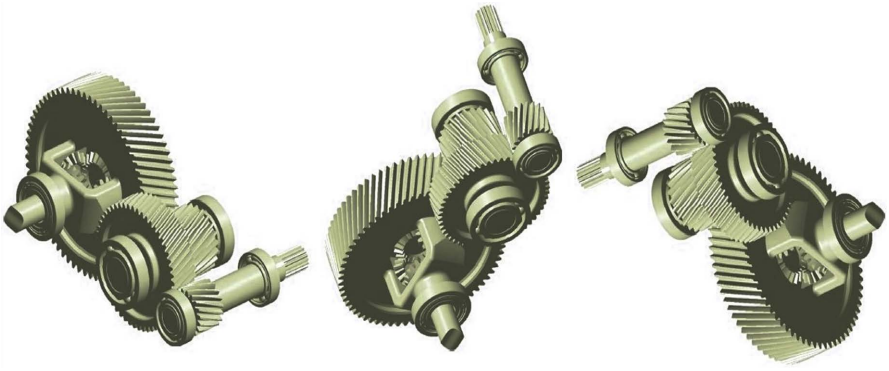

Figure 2. Designed model for the transmission case.

Table 4. System gear parameters (differential).

Attributes (Parameters)	Shaft Gear Axle	Planetary Gear
The Number of Teeth	20	16
Module (mm)	3 mm	3 mm
Helix Angle (deg)	51.340 deg	38.660 deg
Reference Diameter (mm)	60	48
Width of the Gear (mm)	12	12
Angular Pressure (deg)	22.3	22.3

planetary gear's estimated spherical radius (R_b) can be calculated using an empirical formula.

$$R_b = K_b \sqrt[3]{T_d}. \tag{12}$$

Furthermore, a specific radius in the shape of a sphere (R_b) was determined to be 31.744 mm, resulting in a range of values for the pitch cone (A_0) between approximately 31.11 mm and 31.43 mm. This range is obtained using the equation $A_0 = (\pi \times 0.98 \times 0.99)/R_b$.

4.1. Design for Transmission Case (Reduced-Weight)

The weight of the vehicle has a direct bearing on the AEV's driving range, which is essential to its development. So, while maintaining safety requirements, using cutting-edge materials and cutting-edge technology can assist lower the weight of the vehicle. With this strategy, the driving range is increased, and dynamic and economical performance are both enhanced. The largest gear in the transmission box, Gear 4, had its weight drastically reduced to 12.725 kg thanks to improved design, underscoring the significance of lightweight design concepts.

4.2. The Design Methodology (Light-Weight)

Conventional principles of mechanical design guided the gear design, with a specific emphasis on considering the root bending fatigue limit and contact fatigue limit of the tooth surface. However, the utilization of overly conservative

safety coefficients often led to unnecessary redundancy in the size of the gears [1]. The material 20CrMnTi, chosen for this study, demonstrates an impressive tensile strength exceeding 1080 MPa, providing ample opportunities for size optimization. While gears typically consist of a hub, rim, and web, Gear 4 deviated from this structure due to its connection with the differential, resulting in limitations for weight reduction. Consequently, the primary focus of the optimization efforts centered on Gear 4 [12], involving the reduction of the gear width coefficient and enhancements in the spoke type. Within the transmission case, the initial coefficient of face width was established at 0.7, corresponding to a face width of 55 mm. However, the target coefficient of face width was adjusted to 0.56, resulting in a reduced face width of 44 mm. Adhering to conventional gear design principles, this adjustment necessitated a reference diameter for Gear 3, which meshes with Gear 4, exceeding 42.35 mm, along with a minimum module size of 2.192 mm, to meet the requisite strength requirements. Consequently, the gear satisfied the specified strength criteria. As a result, the primary objective of this study revolved around enhancing and evaluating the spoke type of Gear 4 to achieve a lightweight design [7] [9].

4.3. Gear Structuring and Design (Light-Weight)

With a focus on structural considerations, the optimization design of the entire transmission system prioritized Gear 4, which accounted for a significant proportion of the weight. This involved reducing the tooth width coefficient and optimizing the spoke structure. The principle of optimal design revolved around two key aspects: ensuring strength requirements were met and preventing the occurrence of resonance during the operation of the transmission gears, as determined through modal analysis. To achieve a lightweight design, the gears underwent progressive optimization using finite element analysis conducted with ANSYS. The main process included the following steps:

1) *Web Thickness Reduction*

Standard classifications for gear structures include spoke, web, and solid. Gear 4 used a web structure and had a reference diameter of 217.4 mm, as was discussed in Section 3.3.1. The web thickness must meet the requirements of mechanical design and be at least 10 mm. These principles led to the web structure being defined as having a thickness of 13 mm, as seen in **Figure 3**.

2) *Web Topology-Optimization*

Topological optimization is a process that involves exploring the most efficient distribution of materials within a designated design area to withstand applied loads effectively. By employing this technique, the stress distribution on the gear's web during operation can be analyzed efficiently, leading to the identification of an optimized material distribution scheme. This approach enables the identification of areas within the system that can be optimized for lightweight design. The topological optimization process typically involves several steps. The selection of acceptable gear materials comes before the building of a finite ele-

ment model. Ansys/Workbench is used to obtain the topological optimization results once the model has been exposed to the necessary loads and boundary conditions. The use of Ansy/Workbench for gear topology optimization has been studied by academics like Huang *et al.* The gear's web's outer section has a high residual strength, according to their research, making it a strong option for lightweight design when hollowing techniques are applied [13].

4.4. Further Analysis

Additionally, spoke-plate gears experience lower equivalent stress compared to structures with circular holes made from the same material. Building on these insights, six through-holes were introduced on the outer section of the web, with each through-hole having an individual area of 9.932 cm^2, resulting in a total through-hole area of 59.592 cm^2. Figure 4 presents a precise illustration of the structure. After examining the dedendum bending stress, it was discovered that the location of the through holes had the maximum stress during gear engagement.

To solve this problem, the model was split into mesh sections, and forces were applied axially, circumferentially, and radially on the through-hole's addendum circle (Figure 5). Figure 6 demonstrates that the maximum stress on the tooth surface was 554 MPa, which is below the allowed limit of contact stress for 20CrMnTi material (745 MPa). However, in Gear 4, a stress concentration of around 130 MPa was seen at the base of the differential shell and the inner ring of the web. This suggests the potential for additional improvements by taking into account the unique material features. The maximum displacement of 0.0997 mm did, however, occur on the tooth surface where the force was applied,

Figure 3. Model after reduction of the web thickness.

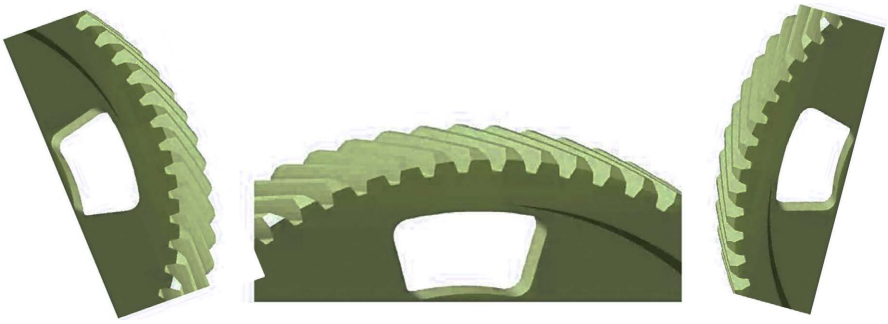

Figure 4. Model of the through-hole.

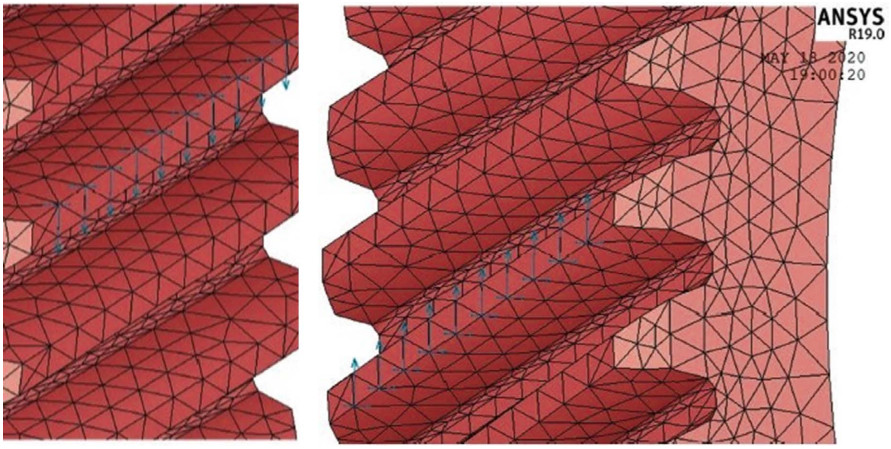

Figure 5. Display of the applied force.

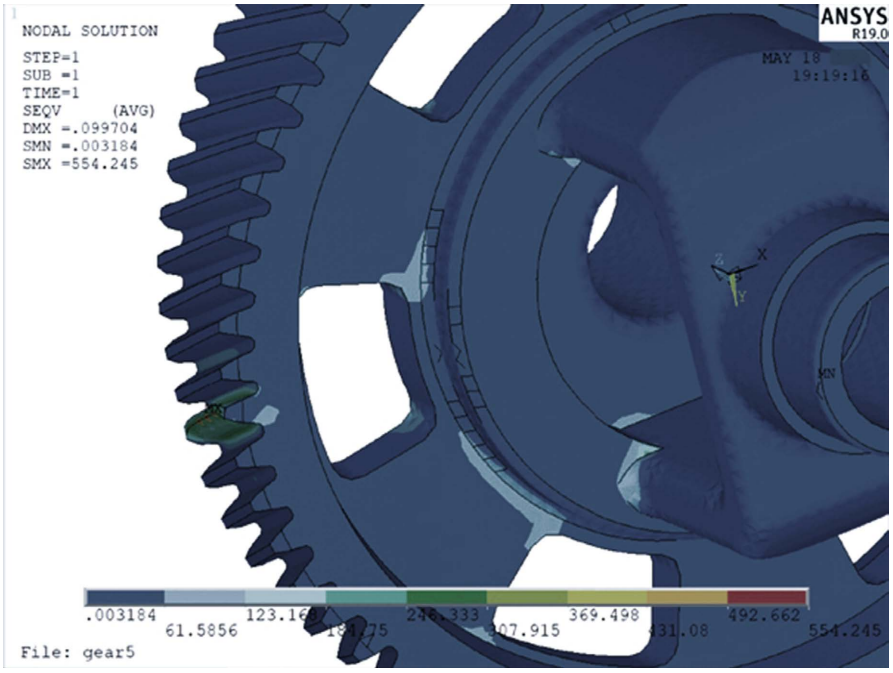

Figure 6. Stress nephogram simulated result.

meeting the required safety standards, as shown in Figure 7.

As previously mentioned, the stress on the web remained well below the limit when six through-holes were present. To explore further possibilities, additional through-holes were studied, resulting in a total of eight through-holes. The combined area of these eight through-holes amounted to 79.456 cm^2. Figure 8 and Figure 9 show the related stress distribution and displacement contour, respectively. Figure 8 shows that the inner ring experiences the majority of the stress, which reaches a maximum value of 163 MPa. The inner ring is under more stress as compared to the six-through-hole construction with this upgraded model. In contrast, Figure 9 shows an increased maximum displacement of 0.121 mm. Overall, the structure has undergone enlargement.

In order to increase production and technological viability, it was determined

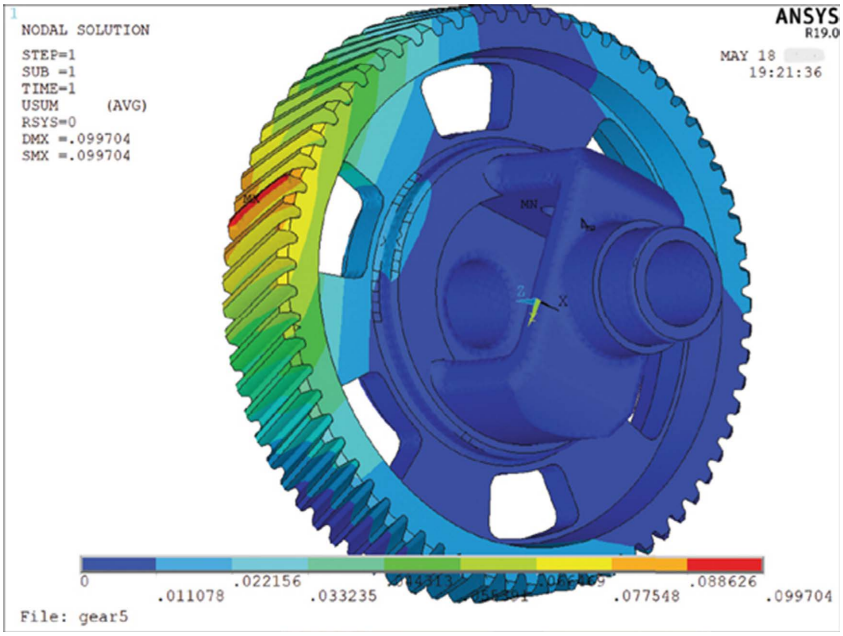

Figure 7. Displaced nephogram simulated result.

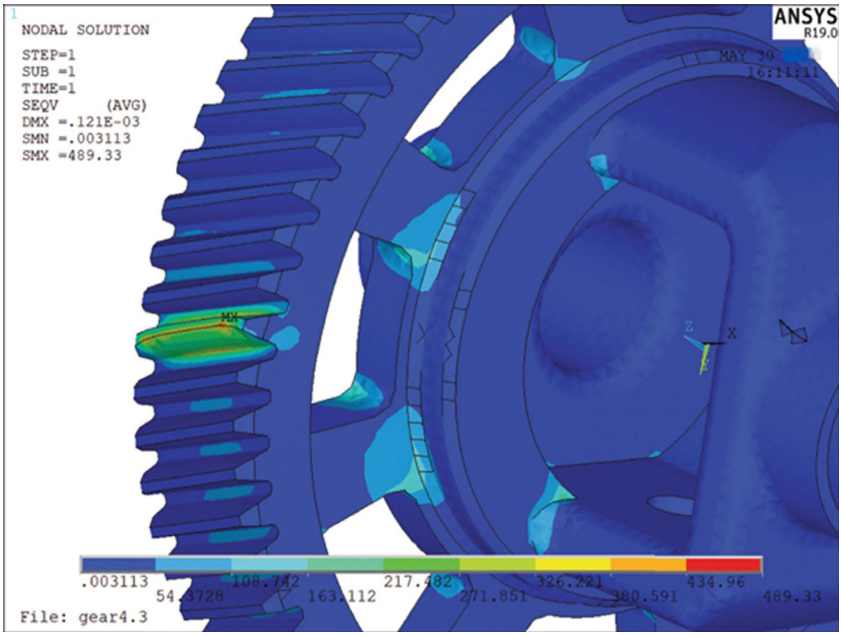

Figure 8. Stress nephogram simulated result.

to reduce the overall number of through-holes while increasing each one's particular area. There were only six through-holes in the simulation, and they each had a bigger area of 15.004 cm^2. As a result, the total area of the through-holes, which was 90.024 cm^2, was more than the area required for the eight-through-hole structure. Under the same circumstances, the maximum displacement reached 0.138 mm and the maximum stress within the web increased to 210 MPa (**Figure 10** and **Figure 11**). This newly optimized lightweight structure meets the required strength criteria.

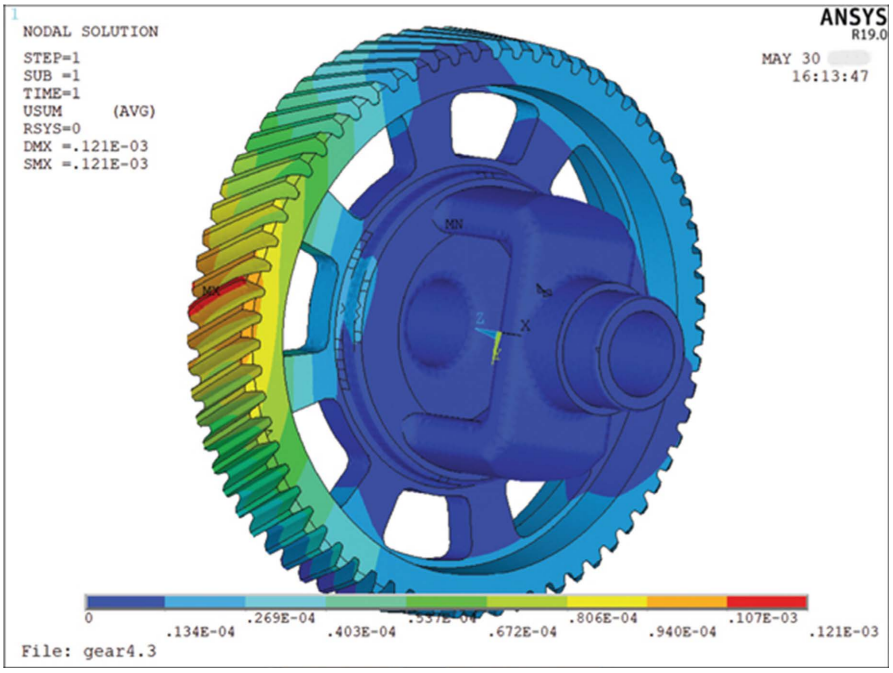

Figure 9. Displaced nephogram simulated result.

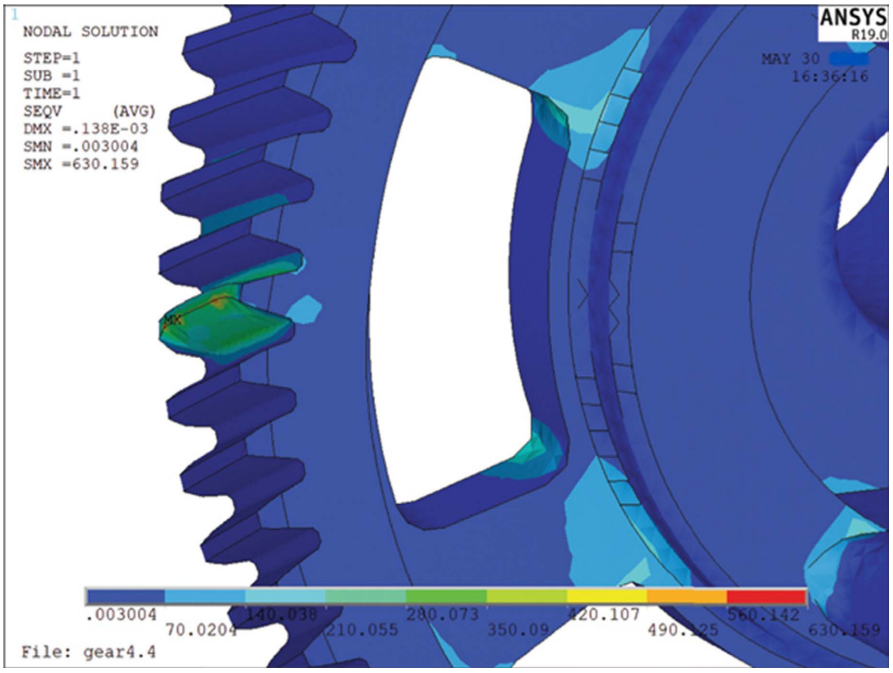

Figure 10. Stress nephogram simulated result.

Following the reduction of the web thickness to the critical size of 10 mm, as recommended in the design manual, the analysis in Figure 12 revealed no significant increase in maximum stress on the web. However, there was an expansion in the area subjected to high forces. However, once the thickness was reduced, the maximum displacement rose by 0.171 mm. But it's important to remember that the mechanical design manual and engineering expertise both

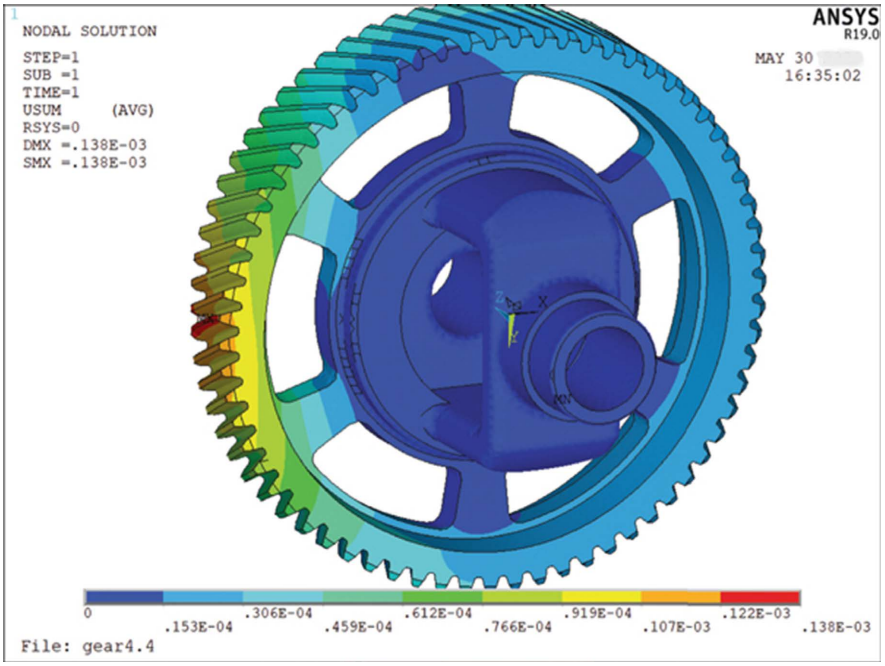

Figure 11. Simulation result of nephogram when displaced.

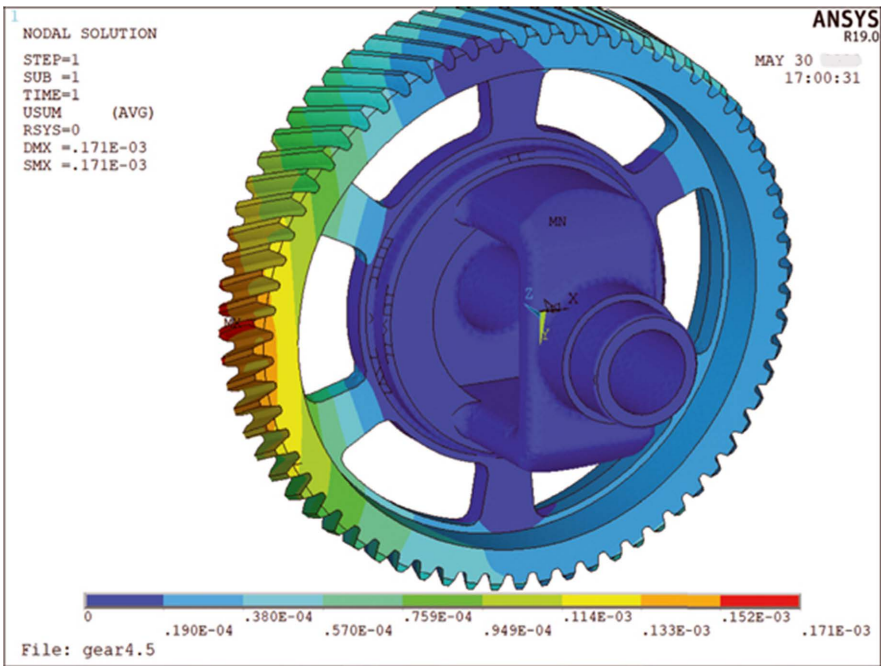

Figure 12. nephogram (stress and displaced) simulated result.

state that the gear deformation shouldn't be greater than 0.15 mm. Consequently, the existing design showed a quite large displacement. As a result, the web thickness was determined to be 13 mm. The finalized structure of Gear 4, incorporating the determined web thickness, is depicted in Figure 13. Its mass was measured in CATIA and found to be 7.498 kg, which represents a reduction of 41% compared to the previous design.

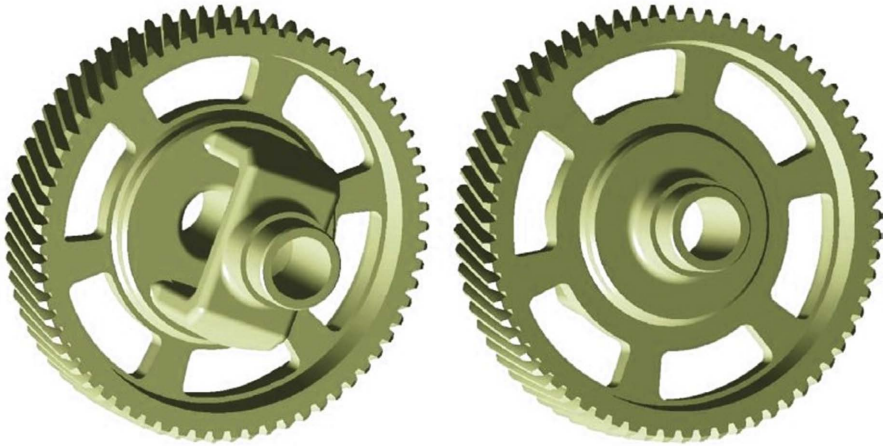

Figure 13. Gear 4 model when optimized.

Table 5. Gear 4-nonupdated modal frequency.

Order	Intrinsic Freq. (Hz)
1	901.22
2	1492.5
3	1924.9
4	2306.2
5	2311.9
6	2351.0
Allowance Factor	+ or −0.5

Table 6. Gear 4-updated modal frequency.

Order	Intrinsic Freq. (Hz)
1	1103.5
2	1208.4
3	1342.8
4	1668.2
5	1768.7
6	1797.2
Allowance Factor	+ or – 0.5

4.5. Performance Optimization of the Gear

The modal frequencies of the lightweight design Gear 4 were analyzed to assess the possibility of resonance. Initially, the six primary modes of vibration were studied for the original gear structure, with restrictions placed on all degrees of freedom at the bearing positions. The corresponding relative modal frequencies were recorded and presented in Table 5.

Subsequently, the same analysis was performed on the updated gear structure, and the results are presented in Table 6. Upon comparing the updated structure with the original one, minimal differences were observed in the modal frequencies. However, notable variations were noticed in the mode shapes for the last three modes. The first mode exhibited an increased natural frequency, while the remaining modes experienced a slight decrease. Importantly, all the modal frequencies remained within a safe range that would typically not induce resonance.

5. Conclusion

In summary, this paper focused on the architecture and optimization of the gear system in the retarder unit of compact autonomous electric vehicle (AEV) transmissions. The optimization procedure involved implementing a 20% reduction in face width and introducing a novel spoke configuration. To assure the gear system's safety and dependability, the structural integrity of the gear system was evaluated using finite element analysis. After thorough CATIA analysis, the initial design's total weight of 12.725 kg was drastically decreased by about 41%. As a result, the gear system's final weight of 7.489 kg was achieved, thereby achieving the goal of a lightweight design with the best safety considerations [14]. Moving forward, there are two fundamental areas that warrant further exploration. Firstly, there is a compelling need to investigate the optimization potential of the overall transmission case structure by incorporating cutting-edge materials and advanced manufacturing techniques, aimed at achieving further weight reduction. Secondly, targeted enhancements and updates can be implemented in the device structure integrated within the transmission case, focusing on enhancing transmission power and improving overall efficiency. By comprehensively addressing these aspects, a model system can be developed to maximize the performance of the transmission case, offering superior alternatives for the overall transmission system [15].

6. Future Development

The implementation of a two-stage retarder with strengthened components and advanced topology optimization holds great promise for enhancing system performance and efficiency. This development focuses on reinforcing critical elements such as the high-speed shaft, low-speed shaft, gears, and differential to improve the system's ability to handle maximum torque and ensure long-lasting durability. Advanced topology optimization techniques optimize the design and material distribution, reducing weight while maximizing strength and performance. Integrating a two-stage retarder offers additional benefits, including more precise control of deceleration, leading to improved braking performance and stability. The combination of reinforced components and advanced optimization techniques contributes to increased efficiency, reduced wear, and tear, and enhanced overall system reliability. Embracing these advancements can significantly enhance system performance and efficiency, providing a system that is

better equipped to handle demanding torque requirements and deliver long-term reliability [16] [17].

Conflicts of Interest

The authors declare no conflicts of interest.

References

[1] Ning, X., Zheng, S., Wang, Y. and Feng, J. (2019) Lightweight Design of Gears in the Wheel-Side Reducer Based on Shanghai Road Driving Cycle. *Proceedings of the Institution of Mechanical Engineers, Part D: Journal of Automobile Engineering*, **233**, 1586-1600. https://doi.org/10.1177/0954407018768176

[2] Wang, Y. and Sun, D. (2014) Powertrain Matching and Optimization of Dual-Motor Hybrid Driving System for Electric Vehicle Based on Quantum Genetic Intelligent Algorithm. *Discrete Dynamics in Nature and Society*, **2014**, Article ID: 956521. https://doi.org/10.1155/2014/956521

[3] Wu, Z., Zhu, M., Guo, Y., Sun, L. and Gu, Y. (2021) Drive System Design for Small Autonomous Electric Vehicle: Topology Optimization and Simulation. *Wireless Communications and Mobile Computing*, **2021**, Article ID: 7192484. https://doi.org/10.1155/2021/7192484

[4] Xu, X.Y. (2017) Development of Transmission Technology for Energy-Saving Vehicles and New Energy Resource Vehicle. *Journal of Automotive Safety and Energy*, **8**, 323-332. (In Chinese)

[5] Chen, P.-T., Pai, P.-H., Yang, C.-J. and Huang, K.D. (2019) Development of Transmission Systems for Parallel Hybrid Electric Vehicles. *Applied Sciences*, **9**, Article No. 1538. https://doi.org/10.3390/app9081538

[6] Zhang, B.H. (2017) Parameter Matching Design and Optimization of Power System for Pure Electric. Chongqing Jiaotong University, Chongqing. (In Chinese)

[7] Li, J. (2017) Paremeters Design and Optimization of Powertrain for Battery Electric Vehicle. Chang'an University, Xi'an. (In Chinese)

[8] Ajao, Q.M. (2019) A Novel Rapid Dispatchable Energy Storage System Model Using Autonomous Electric Vehicles to Reduce Grid Dependency. Georgia Southern University, Statesboro. https://digitalcommons.georgiasouthern.edu/etd/1936/

[9] Wang, J.M. (2019) Design and Optimization of Driving System of Battery Electric Vehicle. Jilin University, Changchun.

[10] Wang, P., Gao, S., Li, L., Sun, B. and Cheng, S. (2019) Obstacle Avoidance Path Planning Design for Autonomous Driving Vehicles Based on an Improved Artificial Potential Field Algorithm. *Energies*, **12**, Article No. 2342. https://doi.org/10.3390/en12122342

[11] Ajao, Q.M., Sadeeq, L.G., Casady, A. and Prio, M.H. (2023) Drivers of Mobile Payments Acceptance: The Impact of Networks Externalities. Preprints.org 2023, Article ID: 2023051555. https://doi.org/10.20944/preprints202305.1555.v1

[12] Ajao, Q.M., Haddad, R.J. and El-Shahat, A. (2019) Comparative Analysis of Residential Solar Farm with Energy Storage between the USA and Nigeria. 2019 *SoutheastCon*, Huntsville, 11-14 April 2019, 1-8. https://doi.org/10.1109/SoutheastCon42311.2019.9020420

[13] Hu, J., Ran, H., Pang, T. and Zhang, Y. (2016) Parameter Design and Performance Analysis of Shift Actuator for a Two-Speed Automatic Mechanical Transmission for

Pure Electric Vehicles. *Advances in Mechanical Engineering*, **8**, Article ID: 1687814016664257. https://doi.org/10.1177/1687814016664257

[14] Ajao, Q.M. (2023) Overview Analysis of Recent Developments on Self-Driving Electric Vehicles. Preprints. https://doi.org/10.20944/preprints202305.0248.v1

[15] Takano, K., Nozaki, K., Saito, Y., Negishi, A., Kato, K. and Yamaguchi, Y. (2000) Simulation Study of Electrical Dynamic Characteristics of Lithium-Ion Battery. *Journal of Power Sources*, **90**, 214-223.

[16] Ajao, Q.M., Oludamilare, O. and Sadeeq, L. (2023) Drivers of Mobile Payment Acceptance: The Impact of Network Externalities in Nigeria. *Open Access Library Journal*, **10**, e10240. https://doi.org/10.4236/oalib.1110240

[17] Ajao, Q.M. and Sadeeq, L. (2023) Dynamic Cell Modeling of Li-Ion Polymer Batteries for Precise SOC Estimation in Power-Needy Autonomous Electric Vehicles. ArXiv: abs/2306.10654.